Propagation properties of Bessel beam from right handed material to double negative material slab system

LONG JIN[*], XINGQIANG ZHANG
Department of Basic Science, Hubei University of Automotive Technology, 167 Checheng West Road,
Shiyan City 442002, Hubei province, China

Based on light transfer matrix and Collins integral equation, the evolution of first-order Bessel beam's normalized intensity distribution on emergent surface, its side transmission view in cascaded slab system with three negative refractive index parameters of Double negative material (DNM) including lossless and losses are discussed. Results show that the original incident Bessel beam can reappear in a certain of location by using lossless periodic slab system with negative index materials as long as the negative refractive index n_l=- n_r and each DNM unit length *L=Z, or quasi-periodic slab system while $n_l \neq$ -n_r.* As to losses periodic slab system contained DNM, larger the damping factors γ_e and (or) γ_m are, more serious Bessel beam deformation is formed. we also propose a ring resonator sensor to measure the concentration of starch solution under the rules of above beam transmission theories, functional relation between normalized maximum intensity of emerging Bessel beam and starch solution concentration are investigated by fit linear method, and the curve assuredly reaches to high precision and linearity. It is expected that the proposed ring resonator sensor and the corresponding conclusions can be useful for precise optical measurement, especially for food safety inspection.

1. Introduction

Four-mode differential laser gyro (FMDLG) is one of the significant sensors in inertial navigation guidance, of which the cavity structure is made up of ring resonator [1]. In order to achieve high sensitivity, high-precision and wide-dynamic range measurement, two beams that split by rotatory components and formed a certain frequency interval modes are operated in ring resonator [2]. These beams usually are Gaussian models. However, the field distortion of Gaussian beam caused by diffraction effect always occurs when wave propagates in free space or medium surface, which restricts Gaussian beam's application [3]. For the past few years, much interest has been exhibited in the propagation and characterization of non-diffraction beams [4-5]. Bessel beam, which makes up one of the families of non-diffracting waves, was firstly proposed by Durnin in 1987 [6]. The analytical solution of Bessel beam was obtained by solving the time-independent Helmholtz equations or the Maxwell equations [7]. The remarkable properties of Bessel beam are self-accelerating, self-breathing, self-reconstructing and symmetric, non-spreading central main lobe [7-8]. Zeroth-order Bessel beam has a large bright center intensity. High order Bessel beams, also known as dark-hollow beams, whose center intensity is zero but possess angular momentum [9], which is very useful in precise optical detection, optical coherence tomography,

charged particles and neutral atoms guidance, optical trap (optical tweezers) and optical micro operations [10-12].

Meanwhile, considerable attention has also been paid to metamaterials so-called negative index materials (NIMs) [13-15]. Double negative material (DNM) [16] with simultaneous permittivity ε and permeability μ sometimes is known as left handed material (LHM), of which the extraordinary electromagnetic (EM) properties was firstly proposed by Velesago [17]. In addition, there is single negative material (SNM) among which only one of the EM parameters is negative; this material includes the mu negative media (MNGM, $\varepsilon>0$, $\mu<0$) and the epsilon negative media (ENGM, $\varepsilon<0$, $\mu>0$) [18-19]. NIMs have many markedly novel phenomena, for example, beam focusing and phase compensation, large negative lateral shift [20], negative refraction EM energy [21], inverse Cerenkov radiation, reverse Doppler Effect and negative reverse pressure [17]. Seeing that NIMs have become a very interesting subject on multilayered structures like photonic crystal fiber in both theoretical and applied research for recent years [22-23], other periodic-structure materials like cascaded slab system [24] contained NIMs may also demonstrate intriguing characteristic and deserve research.

In this paper, we systematically discuss Bessel beam's intensity profiles on emergent intersecting surface, its side view when beam propagates in cascaded slab system. The rest of the letter is organized as follows: firstly, the general

formula of Bessel beam propagating through the paraxial optical system is calculated in the space domain by transfer matrix and the Collins integral. Then, the patterns of first-order emerging Bessel beam's intensity distribution on slab surface are further explored, the side view of this beam propagating in cascaded slab system with three different negative refractive index parameters of DNM including lossless and losses are discussed as well. Furthermore, a ring resonator sensor used to detect concentration of starch solution is designed for what is believed to be the first time. Finally, some important conclusions are summarized.

2. Physical model and formulae

The schematic diagram of the cascaded slab system is shown in Fig. 1. The medium layer with red colour stands for right handed material (RHM) and the light blue is NIM, it has been given that a material with left handed character can only be achieved through dispersion, therefore, we choose isotropic DNM, and its relative permittivity and permeability are given by the Drude model [25]

$$\varepsilon_r(\omega) = 1 - \frac{\omega_{pe}^2}{\omega(\omega + i\gamma_e)}, \qquad (1)$$

$$\mu_r(\omega) = 1 - \frac{\omega_{pm}^2}{\omega(\omega + i\gamma_m)} \qquad (2)$$

where ω_{pe} and ω_{pm} are the electric plasma frequency and the magnetic plasma frequency, respectively, γ_e, γ_m denote the electric and magnetic damping factors. The frequency $v=\omega/(2\pi)$ is measured in 10^2 THz, where ω is circle frequency of the input wave. The length of each DNM unit is L. In general, the formula of DNM's refractive index is expressed as following

$$n_l = -\sqrt{\varepsilon_r(\omega) \cdot \mu_r(\omega)} \qquad (3)$$

With regard to RHM, the refractive index and the length of each unit are n_r and Z, respectively.
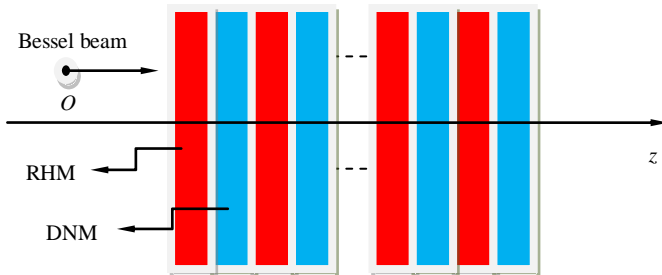
Fig. 1. Light path schematic diagram of cascaded slab system contained DNM

Consider a cluster of high order Bessel beam propagating from O point along the direction of arrow line, the wave electric field at $z=0$ (O point) plane can be described [26-27]

$$E(r_1, \theta_1, z = 0) = J_n(\alpha r_1) \times \exp(-\frac{r_1^2}{\omega_0^2}) \times e^{-in\theta_1} \qquad (4)$$

where $J_n(.)$ denotes the nth-order Bessel polynomial, n is the order of Bessel polynomial, r, θ and z are the radial, azimuthal and longitudinal components, respectively. α denotes the radial wave vector, ω_0 is beam waist and $e^{in\theta}$ is the phase term of the beam, it is obvious that each order Bessel beam behaves circular distribution, only the $e^{in\theta}$ across the annular spectrum can distinguish different orders of them. The propagation of Bessel beam through paraxial optical system can be calculated by the Collins integral

$$E(r_2, \theta_2, z) = (-\frac{i\lambda}{B}) \exp(ikz) \iint_{s_1} E(r_1, \theta_1, z = 0)$$

$$\exp\{\frac{ik}{2B}[Ar_1^2 + Dr_2^2 - 2r_1r_2\cos(\theta_1 - \theta_2)]\}r_1 dr_1 d\theta_1 \qquad (5)$$

where λ=632.8 nm is the input wave length, $k=2\pi/\lambda$ is the wave number. A, B, C and D are the transfer matrix elements of the total paraxial optical systems T, and

$$T = \begin{pmatrix} A & B \\ C & D \end{pmatrix} \qquad (6)$$

Let us introduce now some useful transfer matrices of basic optical medium, e.g. [26, 28]

$$M(x) = \begin{pmatrix} 1 & x \\ 0 & 1 \end{pmatrix} \qquad (7)$$

denotes transfer matrix of wave traveling x distance in the air.

When beam propagates from RHM into DNM slab, the transfer matrix form in RHM-DNM interface can be written as

$$M(n_r, n_l) = \begin{pmatrix} 1 & 0 \\ 0 & \dfrac{n_r}{n_l} \end{pmatrix} \qquad (8)$$

In the same way, DNM-RHM interface transfer matrix is

$$M(n_l, n_r) = \begin{pmatrix} 1 & 0 \\ 0 & \dfrac{n_l}{n_r} \end{pmatrix} \qquad (9)$$

$$R(f) = \begin{pmatrix} 1 & 0 \\ -\dfrac{1}{f} & 1 \end{pmatrix} \qquad (10)$$

denotes transfer matrix of wave reflecting off a concave mirror, where $f=r/2$ indicates focal length of concave mirror, and r is its curvature radius.

By cross-producing those transfer matrices in accordance with the order of the wave propagating from air to the cascaded slab system, we obtain the general formula of Bessel beam propagating through the paraxial optical system in space domain

$$E(r_2,\theta_2,z)=(-\frac{i\lambda}{B})e^{ikz}\,e^{-in\theta_2}\,\frac{\pi}{\frac{1}{\omega_0^2}-\frac{ikA}{2B}}\times \tag{11}$$

$$\exp[\frac{ikDr_2^2}{2B}-\frac{\alpha^2+(kr_2/B)^2}{4(1/\omega_0^2-ikA/2B)}]\times J_n(\frac{k\alpha r_2}{2B(-i/\omega_0^2-kA/B)})$$

and the beam intensity is easily gained by using complex conjugate of $E(r_2,\theta_2,z)$

$$I=\frac{n}{2c\mu_0}\,|\,E(r_2,\theta_2,z)\,|^2\propto|\,E(r_2,\theta_2,z)\,|^2 \tag{12}$$

where c is the speed of light in vacuum.

3. Results and discussion

The first-order Bessel beam normalized transverse intensity distribution profiles before and after wave passing through cascaded slab system $(AB)_m$ with three negative refractive indexes are depicted in Fig. 2, here A and B stand for RHM and DNM, respectively, $m=2$ is the period number of cascaded slab system. Firstly, lossless DNM is chosen and its related parameters are set as $\gamma_e=\gamma_m=0$. we assume $\omega_{pe}=\omega_{pm}=2\pi v\times\sqrt{2}$, $2\pi v\times\sqrt{2.55}$ and $2\pi v\times\sqrt{3.1}$, where $v=c/\lambda=4.74\times10^{14}$Hz, which result in corresponding refractive indexes n_l=-1.00, -1.55 and -2.10, respectively. n_r=1.55 is kept constant, ω_0=0.1 mm, the Rayleigh length of the beam is $Z_R=\pi\omega_0/\lambda$=4.9646 cm, $L=Z=2.5\,Z_R$ fixed. By making a comparison of Fig. 2(a) and (b), it is clearly seen that the incident Bessel beam and emerging Bessel beam's normalized transverse intensity distribution profiles are exactly alike when cascaded slab system contained DNM's abs(n_l)= n_r=1.55. While n_l=-2.10, the emerging beam's maximum intensity decreases to about 0.25 times of the incident Bessel beam seen from colour bar of Fig. 2(c). As to n_l=-1.0 in Fig. 2(d), not only the emerging beam's maximum intensity decays rapidly, but also the spot size more than threefold increases on

emergent surface, hence, the transmission beam quality is the worst of all.
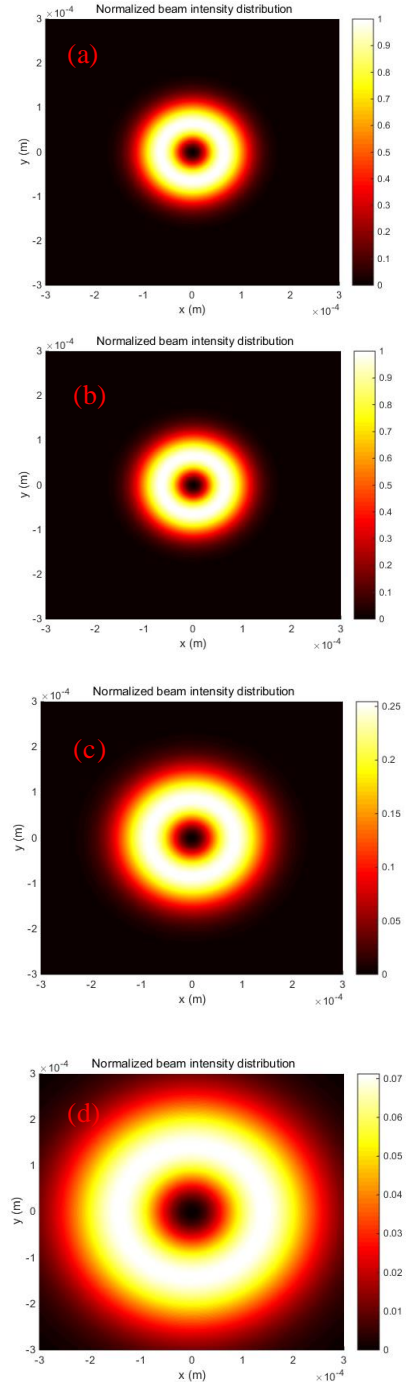
Fig. 2. *High order Bessel beam intensity profiles before and after wave passing through cascaded slab system $(AB)_m$ versus three negative refractive indexes with n=1, α=2.4048 $\times$ $10^4 m^{-1}$, ω_0=0.1 $\times$ $10^{-3}m$, n_r=1.55, Z_R =4.9646cm, L=Z=2.5Z_R and λ =632.8nm fixed. (a) incident Bessel beam distribution, (b) emerging Bessel beam distribution, DNM's $\omega_{pe}=\omega_{pm}$= $2\pi v\times\sqrt{2.55}$ (c) emerging Bessel beam distribution, DNM's $\omega_{pe}=\omega_{pm}=2\pi v\times\sqrt{3.1}$, (d) emerging Bessel beam distribution, DNM's $\omega_{pe}=\omega_{pm}$= $2\pi v\times\sqrt{2}$*

The intensity evolution of first-order Bessel beam propagating in cascaded slab system $(AB)_2$ is deeply investigated in order to show how wave transfers from RHM to DNM, we mainly display the side view of Bessel beam propagating in $(AB)_2$ changed with three negative refractive indexes in Fig. 3, the arrow lines show different material boundaries. It is easily found from Fig. 3(a) that the central dark core of Bessel beam is propagation invariant over a finite distance at begin, and diverges in the rest of first RHM; negative refraction would occur when beam passes through the RHM-DNM interface, that is to say, both incident beam and refracted beam are on the same side of the interface normal; then beam converges in the next DNM, and gets back to its original pattern at the first end of DNM, this phenomenon is called Bessel beam divergence caused by each RHM can just be compensated by the right adjacent DNM, in other words, the incident Bessel intensity profile and emerging beam feature are completely the same as long as $L=Z$ regardless of whether period number m is, related schematic drawing is displayed in Fig. 3(b). while $n_l=-2.10$ and $L=Z=2.5\,Z_R$ in Fig. 3(c), beam divergence when traveling in each RHM cannot be absolutely compensated by the following DNM, therefore, the emerging beam's maximum intensity decreases along with increasing of period number m. Now an urgent issue naturally arises: How long the DNM is needed to just compensate beam divergence when $n_l=-2.10$?

The required length of DNM to exactly compensate divergence in RHM can be calculated through light transfer matrix, when Bessel beam cuts through the first RHM and DNM, the transfer matrix T can be described as

$$T = \begin{pmatrix} A & B \\ C & D \end{pmatrix} = \begin{pmatrix} 1 & 0 \\ 0 & n_l \end{pmatrix} \times \begin{pmatrix} 1 & L \\ 0 & 1 \end{pmatrix} \times \begin{pmatrix} 1 & 0 \\ 0 & \dfrac{n_r}{n_l} \end{pmatrix} \times \begin{pmatrix} 1 & Z \\ 0 & 1 \end{pmatrix} \times \begin{pmatrix} 1 & 0 \\ 0 & \dfrac{1}{n_r} \end{pmatrix}$$

(13)

By substituting $Z=2.5Z_R$, $n_r=1.55$, $n_l=-2.10$ into Eq. (13), we obtain the analytical transfer matrix element B

$$B = -\frac{10}{21} \times L + \frac{625 \cdot \pi}{24521}$$ (14)

therefore, the required length for just compensating divergence in each RHM is $L=3.5Z_R$. The side intensity view of Bessel beam propagating in quasi-periodic slab system with $Z= 2.5Z_R$ and $L=3.5Z_R$ arranged alternatively is depicted in Fig. 3(d), an interesting effect observable in this simulation is that the refracted Bessel beam gets back to its original feature at the end of each DNM, showing a very good agreement with our theoretical analysis. Conversely, the necessary length of DNM to just compensate divergence in each RHM when $n_l = -1.00$ is smaller than $2.5Z_R$. After substituting $Z=2.5Z_R$, $n_r=1.55$ and $n_l =-1.00$ into Eq. (13), analytical transfer matrix element B can also be described as

$$B = -L + \frac{625 \cdot \pi}{24521}$$ (15)

thus, the required DNM length of this quasi-periodic slab system is $L=1.7Z_R$, we also display the simulation result of its structural model with $Z= 2.5Z_R$ and $L=1.7Z_R$ arranged alternatively in Fig. 3(f). While $L=2.5Z_R$ fixed, the reappeared original Bessel beam feature bends again in the rest of first DNM seen from Fig. 3(e), as a result, the emerging beam diverges each other at the end DNM of slab system, leading to a severely distorted beam quality. Since ideal Bessel beams could be extended to infinite space and have infinite energy, they are generally unobtainable in the laboratory, whereas, the above discussion provides an efficient way to regulate quasi-Bessel beam by using cascaded slab with different negative index materials.
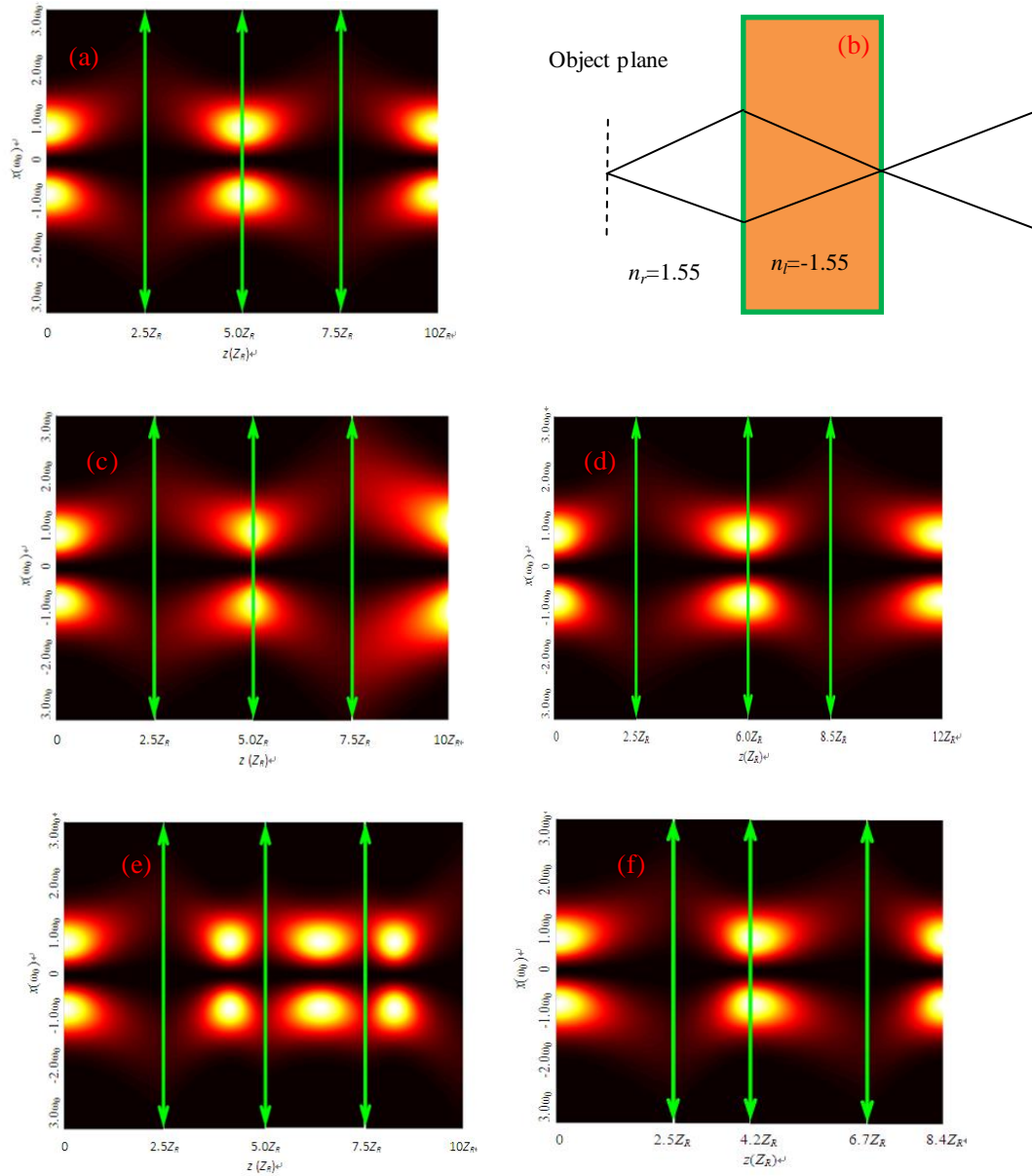
*Fig. 3. Side view of Bessel beam propagating in each RHM and DNM unit successively changed with three kinds of DNMs
(a) DNM's $\omega_{pe}=\omega_{pm}=2\pi v \times \sqrt{2.55}$, (b) principle diagram that beam divergence can just be compensated by each DNM,
(c) DNM's $\omega_{pe}=\omega_{pm}=2\pi v \times \sqrt{3.1}$, (d) Bessel beam transmission in quasi-periodic slab system, $Z=2.5Z_R$, $L=3.5Z_R$,
(e) DNM's $\omega_{pe}=\omega_{pm}=2\pi v \times \sqrt{2}$, (f) Bessel beam transmission in quasi-periodic slab system, $Z=2.5Z_R$, $L=1.7Z_R$*

In practice, losses in DNM are inevitable. In this subsection, the relation between emerging Bessel beam intensity profiles, corresponding side transmission views in cascaded slab system $(AB)_2$ and different damping factors are discussed. We assume $\omega_{pe}=\omega_{pm}=2\pi v \times \sqrt{2.55}$, other parameters are chosen as in Fig. 3, the results are shown in Fig. 4. It is easily acquired that the emerging beam intensity grows steadily worse and spot size enlarges rapidly when beam propagates in each RHM and DNM unit with the increasing of damping factors. When $\gamma_e=\gamma_m=0.01v$, the beam transmission deformation and emerging beam quality are rarely affected from Fig. 4(a) and (b). Whereas, as $\gamma_e=\gamma_m=v$, the maximum emerging

beam intensity decreases to about 0.07 times of the incident beam intensity seen from Fig. 4(e), which manifests beam's attenuation and diffraction of each ring become more and more obvious, thus, It is difficult to ensure remote beam transmission or evolution in optical communication.
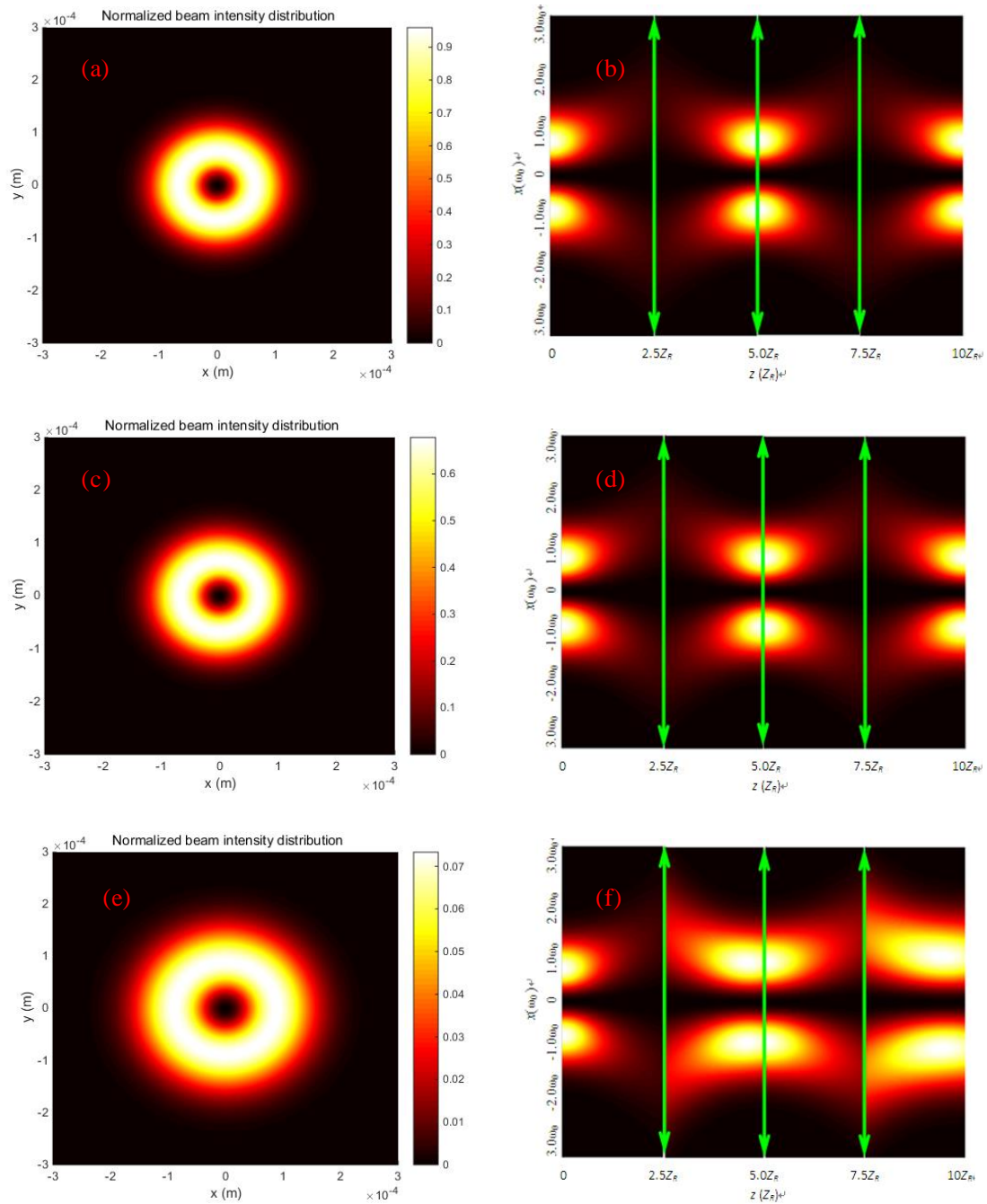
Fig. 4. Emerging beam intensity profiles and corresponding side transmission views with different damping factors, other parameters are chosen as in Fig. 3 except DNM's $\omega_{pe}=\omega_{pm}=2\pi v \times \sqrt{2.55}$ fixed (a) emerging beam intensity profiles, $\gamma_e=\gamma_m=0.01v$, (b) side transmission views, $\gamma_e=\gamma_m=0.01v$, (c) emerging beam intensity profiles, $\gamma_e=\gamma_m=0.1v$, (d) side transmission views, $\gamma_e=\gamma_m=0.1v$, (e) emerging beam intensity profiles, $\gamma_e=\gamma_m=v$, (f) side transmission views, $\gamma_e=\gamma_m=v$

Now, we propose a ring resonator sensor, of which the light path schematic diagram is depicted in Fig. 5 [29], to measure the concentration of starch solution based on the above theories. Mirror A, Mirror B represent plane mirrors and Mirror C, Mirror D are the concave mirrors with curvature radius r=2.5 m. The single cavity length is

l=0.15 m. Active medium with its output wavelength λ=632.8 nm is installed in the center of the two plane mirrors. The cascaded slab system $(AB)_2$ is located in the center of the two concave mirrors, where each A is the space filled with starch solution, B stands DNM with its

$\omega_{pe} = \omega_{pm} = 2\pi\nu \times \sqrt{2.55}$ fixed, $L=Z=0.25Z_R$ in order to match the standard size of ring resonator sensor.
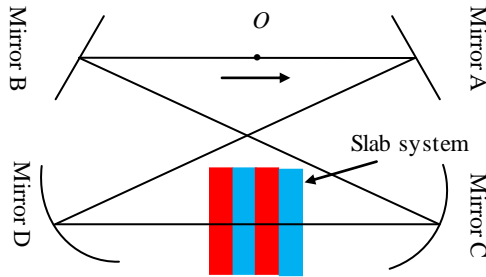
Fig. 5. Ring resonator light path schematic diagram

While Bessel beam propagates a circle from point O along the allow line, the emerging beam intensity distribution on the plane Mirror A cross section when each space A is full of purified water and 20% starch solution are exhibited in Fig. 6. It is clear that the normalized maximum beam intensity to 20% starch solution is bigger than that to purified water seen from color bars of Fig. 6(a) and (b), where the emerging maximum intensity while wave passes through ring resonator sensor with slab unit $n_r=1.55$ is chosen as the normalization coefficient.
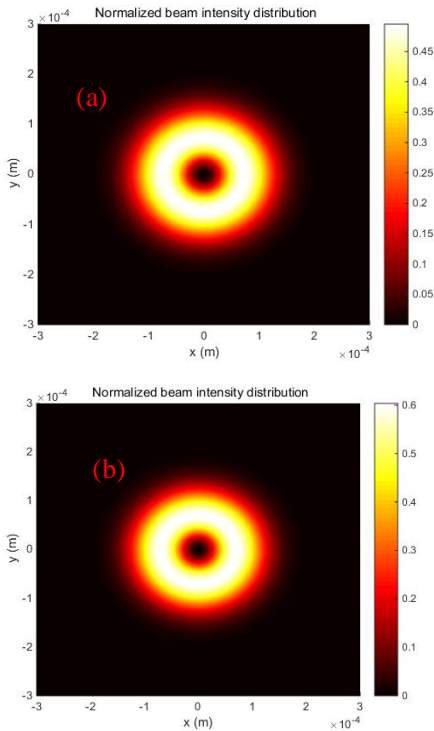
Fig. 6. Emerging intensity distribution on the intersecting plane of Mirror A. (a) emerging beam intensity distribution to purified water, (b) emerging beam intensity distribution to 20% starch solution

In order to have a better understanding of operating principle of this ring resonator sensor, specific analysis is shown as below:

The empirical formula between starch solution concentration and its refractive index is [30]

$$\delta = 572.3 \times N - 762.3 \qquad (16)$$

where N is refractive index of starch solution and δ is solution concentration. When different concentration of starch solution is filled with space A, the relation between normalized maximum emerging beam intensity and solution refractive index is shown in Fig. 7. It is acquired that the normalized maximum intensity gradually becomes bigger while refractive index of starch solution increases, which indicates the starch solution concentration can affect the evolution of the Bessel beams as well like other RHM. Moreover, the curve possesses a good linear property, which provides reliable guarantee for next precise measurements.
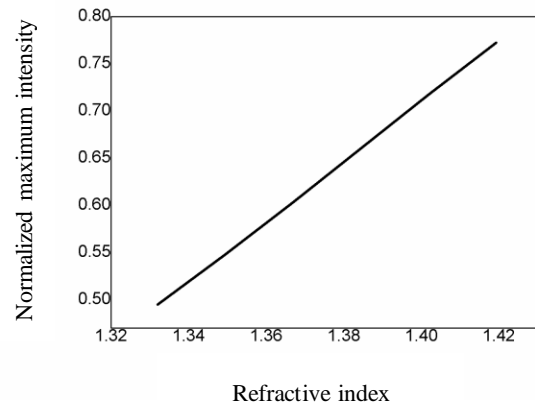
Fig. 7. Relation between normalized maximum intensity and starch solution refractive index. Other parameters are chosen as in Fig. 6
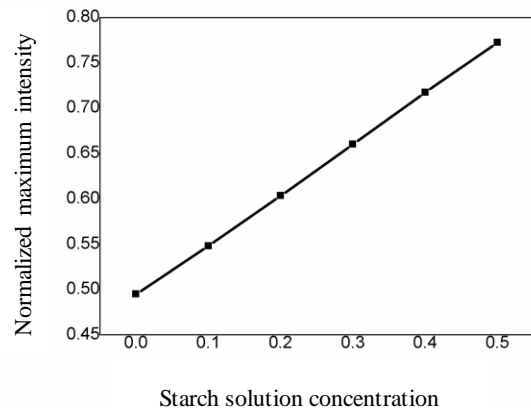
Fig. 8. Relation between normalized maximum intensity and starch solution concentration. Other parameters are chosen as in Fig. 6

The normalized maximum intensity on plane Mirror A cross section changed with different starch solution concentration is explored. The ultimatum is exhibited in Fig. 8, and the curve reaches to high linearity coincidence with our assumption. The mathematical relation between normalized maximum intensity of emerging Bessel beam intensity and starch solution concentration is quantitatively investigated by linear fitting method and the formula is

$$I = 0.49313 + 0.5577 \times \delta \qquad (17)$$

where I signifies the normalized maximum intensity. The statistics of Adjusted R-square and Residual Sum of Squares of the formula are 0.99986 and 6.15626×10^{-6}. As what can be seen from the above parameters and linear equation, this ring resonator sensor demonstrates excellent linear correlation and statistics, we are sure that the rational using of it in concentration detection will become a necessary and useful supplement to chemical sensor.

4. Conclusion

In summary, we have studied the evolution of first order Bessel beam propagating in cascaded slab system $(AB)_2$ contained DNM based on transfer matrix and Collins integral equation. It is revealed that the original incident Bessel beam can reappear in a certain of location by using lossless periodic slab system with negative index materials as long as $n_l = -n_r$ and each DNM unit length $L = Z$, or quasi-periodic slab system while $n_l \neq -n_r$, the conclusion is very important to form stable and excellent beam quality. As to losses periodic slab system contained DNM, larger the damping factors γ_e and (or) γ_e are, more serious Bessel beam deformation is formed. Meanwhile, we have also proposed a ring resonator sensor to measure the concentration of starch solution, of which the operating principle is thoroughly analyzed, the functional relation between normalized maximum intensity of emerging Bessel beam intensity and starch solution concentration is given by Eq. (17), the mathematical results reach to high precision and linearity. It is expected that the proposed ring resonator sensor and the corresponding conclusions can be useful for precise optical measurement, especially for food safety inspection.

Acknowledgements

References

[1] F. Aronowitz, "Fundamentals of the ring laser gyro", Dts, (1999).

[2] S. Zhang, T. Xu, Progress in Nature Science **15**(7), 586 (2005).

[3] X. Cheng, X. Li, Z. Chen, J. Pu, G. Zhang, J. Zhu, High Power Laser Science and Engineering **1**(3-4), 132 (2013).

[4] J. R. Krenn, B. Lamprecht, H. Ditlbacher, G. Schider, M. Salerno, A. Leitner, R. Aussenegg, Europhysics Letters **60**(5), 663 (2002).

[5] S. Wang, X. Mei, X. Xie, F. Wu, Journal of Huaqiao University (Natural Science) **37**(2), 149 (2016) (in Chinese).

[6] J. Durnin, J. J. Miceli, J. H. Eberly, Physical Review Letters **58**(15), 1499 (1987).

[7] J. Zhao, P. Zhang, D. Deng, C. Lou, D. Song, J. Liu, Z. Chen, Chines Optics Letter **11**(11), 110701 (2013).

[8] D. McGloin, K. Dholakia, Contemporary Physics **46**(1), 15 (2005).

[9] X. Zhang, X. Su, L. Zhang, L. Xi, X. Zhang, C. Bai, Chinese Journal of Lasers **41**(12), 113 (2014).

[10] D. G. Grier, Nature **424**(6950), 810 (2003).

[11] M. D. Summers, J. P. Reid, D. McGloin, Opt. Express **14**(14), 6373 (2006).

[12] K. M. Tan, M. Mazilu, T. H. Chow, W. M. Lee, K. Taguchi, B. K. Ng, W. Sibbett, C. S. Herrington, C. T. A. Brown, K. Dholakia, Opt. Express **17**(4), 2375 (2009).

[13] J. Pendry, Physical Review Letters **85**(18), 3966 (2000).

[14] R. Shelby, D. Smith, S. Schultz, Science **292**(5514), 77 (2001).

[15] B. Edwards, A. Alu, M. Silveirinha, N. Engheta, Physical Review Letters **103**(15), 153901 (2009).

[16] D. Smith, W. Padilla, D. Vier, S. C. Nemat-Nasser, S. Schultz, Physical Review Letters **84**(18), 4184 (2000).

[17] V. Veselago, Soviet Physics Uspekhi **10**(4), 509 (1968).

[18] J. Pendry, A. Holden, W. Stewart, I. Youngs, Physical Review Letters **76**(25), 4773 (1996).

[19] J. B. Pendry, A. J. Holden, D. J. Robbins, W. J. Stewart, IEEE Transactions on Microwave Theory and Techniques **47**(11), 2075 (1999).

[20] L. Wang, S. Zhu, Applied Physics Letters **87**(22), 221102 (2005).

[21] W. Lu, J. Sokoloff, S. Sridhar, Physical Review E **69**(2), 026604 (2004).

[22] I. V. Shadrivov, N. A. Zharova, A. A. Zharov, Y. S. Kivshar, Physical Review E **70**(4), 046615 (2004).

[23] P. Li, Y. Lin, Physics Letters A **337**(21), 1870 (2009).

[24] J. Zhou, H. Luo, S. Wen, Y. Zeng, Optics Communications **282**(14), 2670 (2009).

[25] M. W. Feise, Y. S. Kivshar, Physics Letters A **334**(4), 326 (2005).

[26] B. Lü, Laser Optics –beam characterization, propagation and transformation, resonator technology and physics (3rd edition), Beijing: Higher Education Press, 1, 12 (2003) (in Chinese).

[27] X. Lu, X. Chen, L. Zhang, D. Xue, Chinese Physics Letters **20**(12), 2155 (2003).

[28] A. Ghatak, Optics, Beijing: Higher Education Press **5**, 67 (2009).

[29] L. Jin, W. Quan, D. Li, Semiconductor Optoelectronics **35**(2), 363(2014) (in Chinese).

[30] Q. Peng, Z. Zhang, Journal of North University of China (Natural Science Edition) **34**(3), 336 (2013) (in Chinese).

_____
*Corresponding author: crazyjinlong@163.com;
20140007@huat.edu.cn